CHAPTER 219

THE DILUTION PROCESSES OF ALTERNATIVE HORIZONTAL BUOYANT JETS IN WAVE MOTIONS

Hwung, Hwung-Hweng [1], Jih-Ming Chyan [2], Chen-Yue Chang [3], and Yih-Far Chen [4]

Abstract

To investigate the angle effects on the initial mixing processes of the buoyant jet under wave action, the flow visualization and concentration measurements based on laser-induced fluorescence are employed in this study. The dilution improvement of the effluent in the co-wave and opposing-wave is mainly caused by the velocity gradient increasing due to the opposite wave flow and the wave tractive mechanisms resulted from the onshore and offshore wave motion. When orthogonally discharged into wave motions, the effluent is increasingly diluted by the formation of wake vortex and trajectory deflection curved by the wave flow. From the quantitative measurement of tracer concentration, the dimensionless dilution rate shows a function linearly increasing with the dimensionless wave parameter whose coefficient in the orthogonal discharge is above 33% higher than the other two cases. For practical design, it suggests that the orientation of the nozzle should be orthogonal to the propagation of principal wave motion.

Introduction

Ocean outfall has been a feasible alternative of sewage disposal to diminish water pollution problems in most coastal cities. The primary parameter in practical design is the initial dilution rate which should meet the environmental legislation for public health and biological considerations. For the engineers, a simple but accurate method in initial dilution predictions of jet flow discharged into the ocean has been longing for decades. In the past, most relevant researches were theoretically and experimentally conducted in stagnant fluid. However, domestic sewage in the initial mixing processes is affected by oceanographic influences such as currents, density gradients, natural convective processes and wave action. Among these factors, the interaction of jet flow with surface waves is a very fascinating phenomenon in hydrodynamics and also important in the practical design of ocean outfalls.

The subjects concerning the kinematic and dynamic behaviours of jet flow under wave actions were not initiated until Shuto & Ti (1974). It shows that the dilution

[1] Professor, Dept. of Hydraulic and Ocean Engineering. — Director of Tainan Hydraulics Laboratory, National Cheng Kung University, Taiwan, R.O.C.

[2] Associate Researcher of Tainan Hydraulics Laboratory,

[3] Master, Dept. of Hydraulic and Ocean Engineering,

[4] Ph.D. Candidate, Dept. of Hydraulic & Ocean Engineering, Assistant Researcher of Tainan Hydraulics Laboratory.

rate of buoyant plumes in long waves is proportional to the ratio of the discharge velocity to a characteristic horizontal velocity of wave motion, and inversely proportional to the square of the ratio of the water depth to the nozzle diameter. Based on limited experimental results, Ger (1979) suggests that the axial dilution in shallow water waves linearly increase with the dimensionless horizontal distance when it is less than 12. Sharp & Power (1985) observed the dispersion patterns in short waves and long waves respectively, and qualitatively concluded that the short wave would change the jet flow when approaching the surface. The mixing pattern in long waves was obviously affected as soon as the effluent left the nozzle. The above investigations support insufficient information needed in the practical design since most ocean outfalls locate in the intermediate water depth. From the experimental and computational results of of Chin (1987) and Chin (1988), the ratio of the initial dilution rate in intermediate water waves and in still water is shown to be linearly increasing with the ratio of L_q/Z_m. L_q is the spatial scale where the nozzle geometry influences the jet behaviour and Z_m is the length scale required for the wave-induced momentum to be on the same order of the jet momentum. Because of experimental wave conditions being similar to the field situations, the prediction equation proposed is more practicable for the design engineers.

Under the consideration of practicality, however, the interaction mechanisms between the jet flow and surface waves has not been thoroughly understood in the past. Hwung & Chyan (1990) and Chyan & Hwung (1993) investigate a pure momentum jet vertically discharged from the bottom of wave flume and identify the interaction mechanisms, *i.e., jet deflection, wake vortex structure and wave tractive mechanism*, which are responsible for the increase of initial dilution. It also concluded that the jet has a higher dilution ratio when orthogonal to the propagation direction of surface waves. The interaction angle between jets and waves should be an important factor influencing the interaction mechanisms that occur and the sewage dispersion that improves. The purpose of this paper is to investigate discharging angle effects on the mechanisms and the initial dilution of horizontal buoyant jets interacting with surface waves. Avoiding the interference from the direct sampling instruments, the qualitative and quantitative experiments are conducted by an optical method based on laser–induced fluorescence.

Theoretic Considerations

The dilution rate of jet effluents in wave motion is function of the control parameters of the buoyant jets and surface wave, respectively, which includes the factors of the kinematic and dynamic behaviours of buoyant jets such as momentum flux, $M = QV_o$; buoyancy flux, $B = Qg_o$ (effective gravity, $g_o = \frac{\Delta\rho_o}{\rho_o}g$); volume flux, $Q = \pi/4D^2V_o$; and discharging depth, H. In the mentioned parameters, $\Delta\rho_o$ denotes the initial density differences between the effluent and the ambient and ρ_o represents the initial density

of the effluent. The parameter groups describing the motion of surface waves are water depth, h; wave amplitude, a; wave period, T; and gravity, g. There are two more variables describing the relative spatial relationship between the buoyant jet and the surface wave, which are the discharging angle relative to the horizontal plane, θ_1; and the discharging angle relative to the the direction of wave propagation, θ_2. From these control parameters, the characteristics of dilution rate is, then, described as

$$S = f(M, B, Q, H, h, a, T, g, \theta_1, \theta_2) \tag{1}$$

Chin (1987) suggests that the dominant mechanisms influencing the dilution of the effluent may be more easily characterized by formulating the dimensional variables in terms of length scales. As proposed by Fischer *et. al.* (1979), the definitions of appropriate length scales are

$$L_q = \frac{Q}{M^{1/2}} = (A)^{1/2} \tag{2}$$

$$L_m = \frac{M^{3/4}}{B^{1/2}} \tag{3}$$

$$Z_m = \frac{M^{1/2}}{U_{max}} \tag{4}$$

where L_m is the length scale beyond which the buoyancy dominates the plume flow; A denotes the area of the nozzle cross section; and U_{max} is the amplitude of the horizontal wave particle velocity. From the small amplitude wave theory, U_{max} is defined by

$$U_{max} = -\frac{agk}{\sigma \cosh kh} \tag{5}$$

$\sigma = \frac{2\pi}{T}$ and $k = \frac{2\pi}{L}$ are the angular frequency and the wave number, respectively. From the Buckingham π theorem and Eq.(2)~Eq.(4), non-dimensionalizing Eq. (1) with the dilution rate of buoyant jets in still water, S_o, yields

$$\frac{S}{S_o} = f(\frac{H}{L_m}, \frac{L_m}{L_q}, \frac{Z_m}{L_q}, \frac{h}{L}, \theta_1, \theta_2) \tag{6}$$

which contains the non-dimensional variable groups characterizing the dilution enhancement of the effluent under wave action. In most practical conditions, $H \gg L_m \gg L_q$, which indicates that the effluent will be plume–like very quickly after leaving the nozzle. According to the observations of Sharp & Power (1985) and Chyan & Hwung (1993), no strong interaction between the jet flow and wave motion occurs when the axial jet momentum being weak. In fact, H/L_m and L_m/L_q are important dimensionless

parameters influencing S_o, however, they become minor in the dilution improvement effect of wave motion on buoyant jets when $H \gg L_m \gg L_q$. In the present study, $\theta_1 = 0$ and Eq. (6) can be simplified as

$$\frac{S}{S_o} = f(\frac{Z_m}{L_q}, \frac{h}{L}, \theta_2) \tag{7}$$

Chin (1987) suggests that the relative depth, h/L, does not play a significant role in the dilution enhancement. From Eq. (5), Z_m/L_q is not independent of h/L, then, the effect of the latter in the dilution enhancement is implicitly involved in the former. From the experiments conducted by Chin (1987), the relation of Eq. (7) is demonstrated to be a linear function

$$\frac{S}{S_o} = 1 + C_s \frac{L_q}{Z_m} \tag{8}$$

where C_s is a coefficient depending on the interaction angle between the buoyant jet and surface wave. From the quantitative measurement, C_s can be determined to evaluate the characteristics of the angle effect.

Experimental Setup

The nature of surface waves is an unsteady kinematical phenomenon. Optical method based on laser-induced fluorescence (**LIF**) is employed to carry out the flow visualization and the concentration measurements. The technique of **LIF** avoids distorting the interaction flow of jets and surface waves, and is sensitive up to tracer concentration of 0.19 pb. The experiments are conducted in a wave tank of $12m \times 0.5m \times 0.6m$. A piston type wave maker is installed on one end of the wave flume and a wave absorber locates on the other side to diminish the wave energy. Supplied by a constant head assembly, the effluents mixed with tracer is discharged by a nozzle of diameter of 0.33 cm at middle part of wave flume. Three discharge angles of jet flow relative to the propagating wave direction, *i.e.,* 0° (co-wave), 180° (opposing wave), 90° (orthogonal discharge), are selected to investigate the angle effects on the initial dilution processes. In case of orthogonal discharge, the nozzle is located nearby the side wall and otherwise in the centerline of the flume.

Flow Visualization—

Drexhage (1973) found that the dye, Rhodamin 6G ($C_{28}H_{31}C\ell N_2O_3$), could emit yellow fluorescence (wavelength=570 nm) when stimulated by an Argon-ion laser (wavelength= 514.5 nm). If the effluent contains with fluorescent dye, the flow pattern and vortex structures of the jet flow under wave action could be visualized by a sheet of laser light. The installation of flow visualization is shown in Fig. 1 where the laser beam is

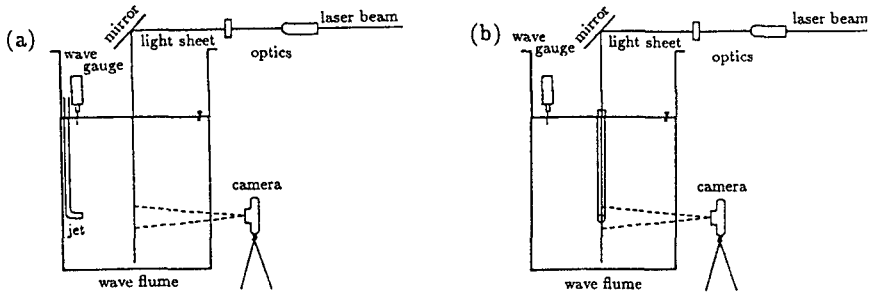

Fig. 1 Experimental layout of flow visualization for cases of (a) orthogonal discharge (b) co-wave or opposing-wave

transformed to a light sheet by an optical system. In order to understand the flow pattern related to the wave phase, signals from the wave gauge and the electrical shutter of the camera are simultaneously collected by the data acquisition system. As shown in Table 1, three cases (Case 1 $\sim$ Case 3) with a lower Reynolds number ($R_e = 772$, $F_d = 7.05$) is employed to clearly visualize the vortex structures. Especially, there is no buoyancy in Case 2 because of the necessity for the observation of wake vortex formed in the interaction process. Strong density difference will seriously distort the image. If the location of laser light sheet is in the zone of flow establishment, pure momentum jet can be employed to simulate the interaction of buoyant jet with surface waves since the momentum force rather than the buoyant force is the dominant force of the flow field.

Quantitative Measurements—

The principle of LIF is also applicable to the quantitative measurements. According to the Lambert–Buoguer–Beer law in Yoe & Koch (1957), the fluorescent intensity, F, can be described by the Taylor series,

$$F = K_1 I_o \left[2.3ecd - \frac{(-2.3ecd)^2}{2!} - \frac{(-2.3ecd)^3}{3!} - \cdots - \frac{(-2.3ecd)^n}{n!} \right] \tag{9}$$

where K_1=proportional coefficient; I_o=intensity of incident laser beam; e=molar extinction coefficient; c=tracer concentration; and d=length of test section. If the tracer concentration is low enough to the have the higher order terms neglected in the equation, the intensity of fluorescence with fixed K_1, I_o, e and d will be a linear function of tracer concentration. A calibration process is able to quantify this characteristic function which, in the following quantitative measurements, transforms the voltage signals from photo-detector into concentration data. Fig. 2 shows an example of calibration

Table 1 Experimental conditions

Case	$\Delta\rho$	D	Q	h	H	T	$2a$	h/L	L_q/Z_m
	σ	cm	cm^3/s	cm	cm	sec	cm		
1	30	0.33	1.9	40	36	1.20	5.80	0.207	0.1187
2	0	0.33	1.9	35	22	1.00	4.00	0.273	0.0527
3	30	0.33	1.9	35	22	1.00	4.00	0.273	0.0527
4	30	0.33	7.7	40	36	0.83	5.32	0.378	0.0527
5	30	0.33	7.7	40	36	0.93	4.83	0.309	0.0626
6	30	0.33	7.7	40	36	1.20	4.66	0.207	0.0892
7	40	0.33	7.1	40	36	0.89	6.51	0.334	0.0827
8	40	0.33	7.1	40	36	1.10	5.72	0.235	0.1060
9	40	0.33	7.1	40	36	1.35	5.70	0.175	0.1210
10	40	0.33	7.1	40	36	1.38	5.48	0.170	0.1182
11	40	0.33	7.1	40	36	1.24	6.85	0.197	0.1356
12	40	0.33	7.1	40	36	1.11	6.01	0.232	0.1049
13	40	0.33	7.1	40	36	1.00	7.45	0.273	0.1122
14	40	0.33	7.1	40	36	0.89	6.35	0.334	0.0753
15	40	0.33	7.1	40	36	0.84	5.87	0.370	0.0589
16	40	0.33	7.1	40	36	1.12	6.30	0.229	0.1099
17	40	0.33	7.1	40	36	0.83	7.25	0.378	0.0723
18	40	0.33	7.1	40	36	0.89	8.09	0.334	0.0957
19	40	0.33	7.1	40	36	1.00	7.04	0.278	0.1060
20	40	0.33	7.1	40	36	1.25	5.64	0.195	0.1120
21	40	0.33	7.1	40	36	1.32	5.95	0.181	0.1329
22	40	0.33	7.1	40	36	0.90	6.39	0.327	0.0834
23	40	0.33	7.1	40	36	1.09	4.99	0.238	0.0914
24	40	0.33	7.1	40	36	1.00	4.83	0.273	0.0779
25	40	0.33	7.1	40	36	0.92	4.16	0.315	0.0575
26	40	0.33	7.1	40	36	0.92	4.75	0.315	0.0656
27	40	0.33	7.1	40	36	1.00	7.57	0.273	0.1220
28	40	0.33	7.1	40	36	1.09	5.55	0.240	0.1014

curves. Three cases, such as pure water ($\rho = 998kg/m^3$, $20°C$); water–alcohol mixture (1:5.33); and pure alcohol (95%, $\rho = 808kg/m^3$, $20°C$), are employed to investigate the effect of compositions. It shows that the slopes are the same except the intercept caused by different system error. Before conducting the concentration measurement in a new test point, the background level of tracer concentration has to determined to rid data of system error. The correlation coefficient of each calibration curve is larger than 0.999 and the standard deviation is lower than 0.1 ppb.

Most ocean outfalls usually locate in the intermediate water depth where the depth-to-wavelength ratio, h/L, ranges from 0.05 to 0.5. On the consideration of prac-

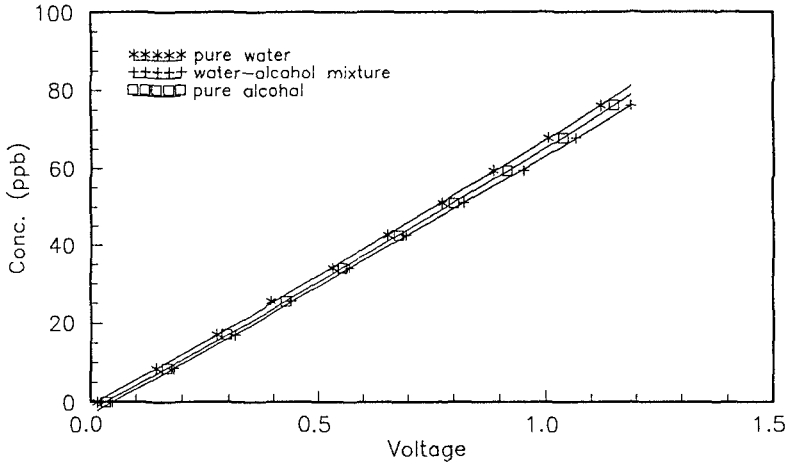

Fig. 2 Calibration curves of different compositions

tical applications, all of experimental conditions are in this range as shown in Table 1. Suitable *Reynolds No.* ($R_e > 2450$) and *Froude No.* ($18.9 < F_d < 23$) are also selected to keep the simulated flow pattern similar to that of the diffusers. According to Chin (1987), the blocking layer of a buoyant jet with a poor dispersive ability is about 10% of the discharge depth. The measuring plane including 5 $\sim$ 7 points locates 5 *cm* under the still water surface. The water surface variations induced by surface waves may block the fluorescence emitted from the measuring point while moving toward a higher test level. With the appropriate experimental conditions, the quantitative measurements of a buoyant jet under the action of surface waves can be proceeded. The data acquisition system collects signals from photo-detector and wave gauge in a sampling rate of 100 *Hz* and sampling duration of 60 *sec*. The initial dilution of different interaction cases can be determined from the experimental data, therefore, quantitative assessment of angle effects can be obtained and applied in the practical design of ocean outfalls.

Results and Discussions

Flow Visualization—

The flow visualization results of buoyant jet in co-wave are shown in Photo 1 where the flow pattern in still water is also pictured in Photo 1(a) for comparison. The trajectory in still water near the nozzle remains horizontal in the momentum-dominant domain, however, it gradually bends as the buoyant force getting stronger. During the ascending period, the effluent mixes with the ambient water and the boundary

(a)

(b)

(c)

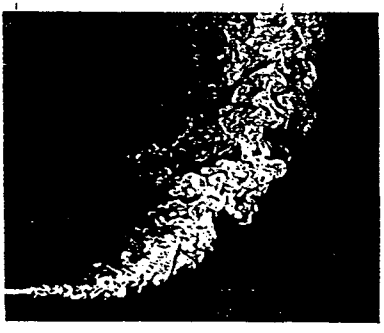

(d)

(e)

Photo 1 Flow of buoyant jets in co-wave (Case 1), (a) still water, $t/T=$ (b) 0, (c) 0.25, (d) 0.49, (e) 0.73.

spreads simultaneously. Obviously, the vortex resulted from the velocity gradient plays an important role in lateral mass transfer and concentration dilution. Concerning the buoyant jet in wave motion, it is classified according to the temporal duration of wave crest and wave trough. The effluent experiences a co-stream flow induced by wave motion in the former while it interacts with an opposing flow in the latter. In case of wave-induced opposing flow, as shown in Photo 1(b), it is interesting to observe that the spreading rate of jet boundary in the neighborhood of the nozzle is larger than that in still water. The horizontal distance from the nozzle to the location where the plume ascending completely upward is shorter in Photo 1(b) than that in Photo 1(a). It shows that the effluent interacts with an opposing and inclining flow induced by wave motion. A greater velocity gradient and the opposing flow explain the formation of an increasing spreading rate and shorter excursion distance. There are many slender and inclining strips of jet fluid near the nozzle. According to Chyan & Hwung (1993), this structure is closely connected to the wake vortex. Due to the buoyancy and the upward wave flow being the same direction, the former will accelerate the formation of wake vortex even if the latter is small. As shown in Photo 1(e) where the opposing wave flow still influencing the effluents, there doesn't exhibit similar structures. It is because that the buoyant force prohibits the formation of wake vortex. From the above discussion, it explains the reason that, as shown in Photo 1(b) $\sim$ Photo 1(e), the slender strips of the effluent always occur in the offshore side of the buoyant jet. This mechanism also changes the symmetry of profile distribution of the buoyant jet. However, these phenomena imply the mechanisms responsible for the increase of dilution rate.

On the phase of wave crest ($t/T = 0.25$), as shown in Photo 1(c), the wave flow near the nozzle is parallel to the jet flow. It results in a smaller velocity gradient which depressing the formation of vortex and spreading rate. When $t/T = 0.49$, the inclining flow contains an upward velocity component, it will be against the ascending tendency of the effluent. As shown in Photo 1(d), there is a region where the trajectory is almost horizontal. Compared to the buoyant jet of the same trajectory characteristics in still water, the length scale in horizontal direction is longer and the spreading rate is smaller. From the observation of the effluent influenced by the co-stream of wave motion, the wave flow during the phase of wave crest seems to diminish the dispersion ability of the buoyant jet. In fact, there is an additional mechanism of dilution improvement during the interaction of co-stream and opposing flow on the effluent. As mentioned in the above discussion, the excursion distance will be shortened by the opposing and upward wave flow and stretched by the co-stream and downward wave flow. When the velocity of buoyant jet being too low to interact with surface waves, the plume will merely oscillate with wave motions which can not change the relative position within the effluent. Sharp & Power (1985) and Chyan & Hwung (1993) had observed the same phenomena. The effluent plumes ascending in the stretched excursion of wave

crest phase will enclose a large volume of ambient water with the following plume in the shortened excursions of wave trough. Therefore, a few patches of fresh water can be found in the ascending effluent plume as shown in Photo 1(b) $\sim$ Photo 1(e). This additional mechanism provides a new chance of dilution and is similar to the wave tractive mechanism found by Chyan & Hwung (1993).

The flow visualization results of buoyant jet oppositely discharged into the wave motion would not be discussed herein since it shows a qualitatively similar result obtained in the co–wave case. Photo 2 depicts the formation cycle of wake vortex on the plane 1.1 *cm* away from the nozzle in the orthogonal discharge case. Within the momentum dominating domain of buoyant jets, it is acceptable to employ a pure momentum jet to simulate the momentum interaction of buoyant jets with surface waves for observing the inside structures of wave vortex. As shown in Photo 2(a) ($t/T = 0$), the appearance of the effluent has been upwardly distorted into a horseshoe by the cross-flow induced by waves. The vertical velocity of intermediate wave is usually smaller than the horizontal velocity. During the wave phase of $t/T = 0$ and $t/T = 0.5$ when the vertical velocity dominates, the vortex induced by wave motion can not develop completely. A pair of counter-rotating vortex are not formed until the cross-flow of wave motion is large enough, as shown in Photo 2(b). As shown in Photo 2(a) $\sim$ 2(f), the axes of vortex pair also rotates clockwise as the wave flow vector does except that the vortex around the phase of $t/T = 0$ or $t/T = 0.5$ is relatively immature. The formation of wake vortex certainly increases the dilution rate due to additional forced entrainment.

In order to investigate the buoyancy effect on the wake vortex formation, the flow visualization experiments of Photo 2 repeat again except the substitute of the pure momentum jet with a buoyant jet. The experimental results are shown in Photo 3 whose images are obscured by the density gradient. From the appearance of the flow structures, the wake vortex can still be found in Photo 3(c). The interacted structures are more sophisticated than that of the momentum interaction as depicted in Photo 2. A curved vortex tail following the wake vortex is observed and it mainly results from the vortex occurred before the test section. From the above observations, it suggests that the buoyancy effect will enhance the unsteadiness of the jet flow. The dispersion area of the effluent is enlarged by this effect, which implies the increase of dilution rate. In fact, the flow field of buoyant jet orthogonally discharged into the wave motion is a very complex but interesting flow phenomenon. In addition to the formation of wake vortex, the jet trajectory deflects in a status of 3-dimensional while a 2-dimensional deflection was observed by Chyan & Hwung (1993). Generally, the jet is onshore and offshore deflected in wave phase of $t/T = 0.25$ and $t/T = 0.75$. In phase of $t/T = 0$, the ascending process of the effluent occurs earlier because of the upward vertical wave velocity while the horizontal domain of the trajectory will be stretched in phase of

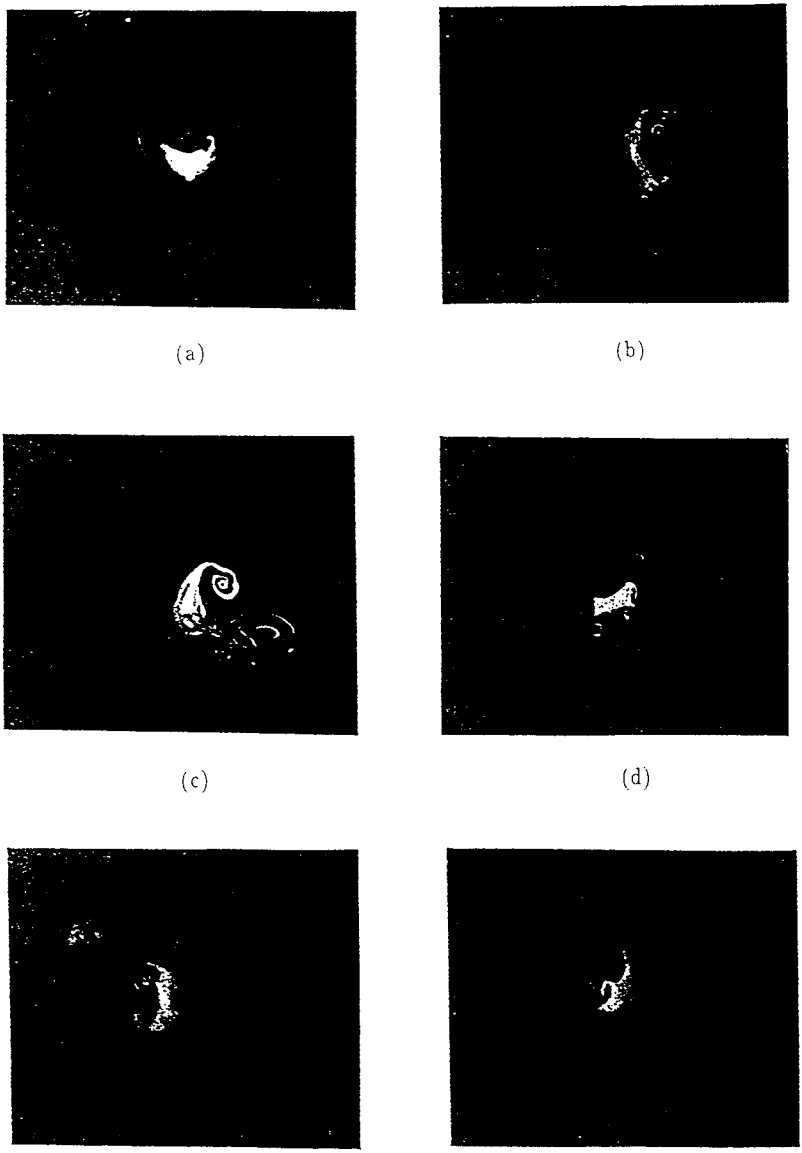

Photo 2 Formation cycle of wake vortex in orthogonal interaction (Case 2)
$t/T=$ (a) 0, (b) 0.21, (c) 0.30, (d) 0.44, (e) 0.65, (f) 0.81.

$t/T = 0.5$. Due to the periodic deflection induced by wave motion, the shape of the effluent plume is no longer a circle, however, the mixing area of the effluent will be increased by the deflection mechanism and wake vortex structures.

From the above discussions, it suggests that the mechanisms improving the dilution rate of the buoyant jet in cases of co-wave and opposing wave result in the velocity gradient increase and wave tractive mechanism. The deflection mechanism and wake vortex structure play an important role in the enhancement of dilution rate when the buoyant jet orthogonally discharged into the wave motion. Concerning the contribution of these mechanisms to the dilution increases, it can only be evaluated by the quantitative measurements which will be discussed in the following.

Dilution Measurements—

From the elaborate measurements of S and S_o, the data obtained was processed according to Eq. (8) and the results of interaction angles, 0°, 180°, and 90°, are shown in Fig.3. The regression relationships of S/S_o and L_q/Z_m are linear as proposed by Eq. (8) which are

$$\text{co-wave} \quad : \quad \frac{S}{S_o} = 1 + 4.21\frac{L_q}{Z_m} \tag{10}$$

$$\text{opposing-wave} \quad : \quad \frac{S}{S_o} = 1 + 4.16\frac{L_q}{Z_m} \tag{11}$$

$$\text{orthogonal discharge} \quad : \quad \frac{S}{S_o} = 1 + 5.55\frac{L_q}{Z_m} \tag{12}$$

with the correlation coefficients being 0.90, 0.93, and 0.91, respectively, while the standard deviations are 0.10, 0.08, and 0.10. Positive slopes indicate the wave action increasing the dispersion of the effluent. From the flow visualization identifying the similar interaction mechanisms in cases of co-wave and opposing wave, it results in the coefficient, C_s, almost equivalent in both cases. As shown in Fig. 3, Chin (1987) suggests a higher estimate of $C_s = 6.15$ which may be because of the sampling method and the calibration relation. The mechanisms, *i.e. wave deflection and wake vortex*, formed in the orthogonal discharge obviously play a more effective role in the dilution enhancement. In coastal water, the propagation of surface waves is not unidirectional so that the orientation of the diffusers can only be designed to be orthogonal to the principal direction which will provide the highest initial dilution. To estimate the dilution rate increased by wave action, the data obtained in different interaction angles is collected in Fig. 4 which shows $C_s = 4.87$.

Conclusion

The mechanisms improving the initial dilution processes of jet flow in co-wave and opposing wave are identified as the velocity gradient increase induced by the opposite

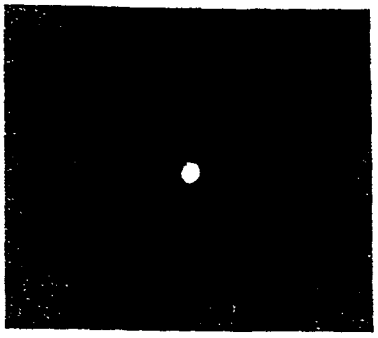

(a)

(b)

(c)

(d)

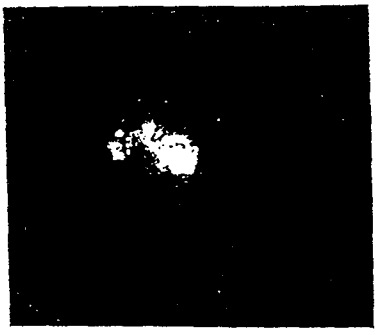

(e)

Photo 3 Buoyancy effect on the formation of wave vortex (Case 3). (a) still water, $t/T=$ (b) 0.08, (c) 0.27, (d) 0.42, (e) 0.88.

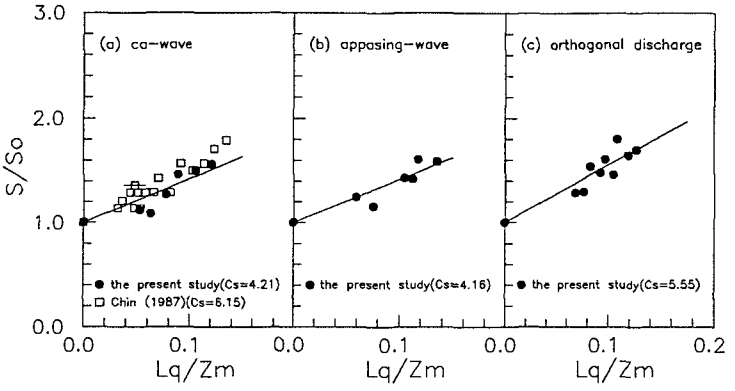

Fig. 3 Angle effects on initial dilution rate of jet-wave interaction
θ_2 = (a) 0°, (b) 180°, (c) 90°

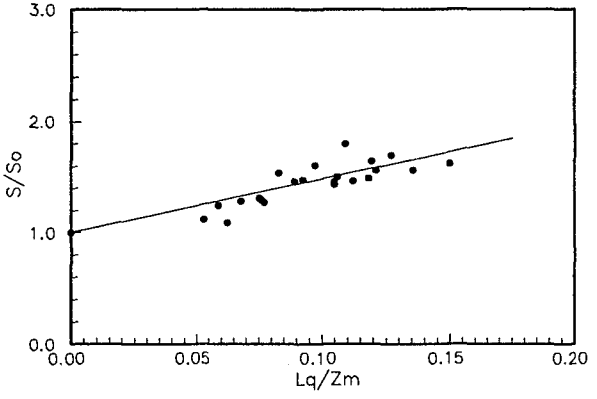

Fig. 4 Estimate of initial dilution increase

wave flow and the wave tractive mechanism stemmed from the onshore and offshore wave flow. When orthogonally discharged into wave motion, the effluent is affected by different interaction mechanisms, such as wake vortex and wave deflection. The concentration measurements show that the increase of the initial dilution is comparable in cases of co-wave and opposing wave. However, a higher increasing tendency is found in the orthogonal discharge whose C_s is 33% larger than that of the other cases. It

implies that the orthogonal discharge is a more effective orientation in the enhancement of mixing efficiency. Considering the field situation in coastal water, an average value of $C_s = 4.87$ is suggested to estimate the dilution rate increase of the buoyant jet under the wave action.

Reference

1. Chin, D.A. (1987), Influence of surface waves on outfall dilution, J. of Hydraulic Eng., Vol. 113, No. 8, pp.1006–1017.
2. Chin, D.A. (1988), Model of buoyant-jet-surface-wave interaction, J. of Waterway, Port, Coastal, and Ocean Eng., Vol. 114, No. 3, pp.331–345.
3. Chyan, J.M. & Hwung, H.H. (1993), On the interaction of a turbulent jet with waves, J. Hydraulic Research, Vol. 31, No. 6, pp. 191-810.
4. Drexhage, K.H. (1973), Structures and properties of laser dyes, Topics in Applied Physics, Springer, Vol. 1, pp. 145-193.
5. Fischer, H.B., List, E.J., Koh, R.C.Y. Imberger, J. & Brooks, N.H. (1979), Mixing in inland and coastal waters, Academic Press, New York, N.Y., U.S.A.
6. Ger, A.M. (1979), Wave effects on submerged buoyant jets, Proc. Hydraulic Eng. in Water Resources Development and Management, IAHR, pp. 295-300.
7. Hwung, H.H. & Chyan, J.M. (1990), The vortex structures of round jets in water waves, Proc. Int'l. Conf. on Physical Modeling of Transport and Dispersion in conjunction with the GARBIS H. KEULEGAN Centennial Symp., IAHR, pp.10A.19–10A.24.
8. Sharp, J.J. & Power, K.C. (1985), The local effect of wave action on submerged effluent discharge, Canadian Coastal Eng., pp.1–10.
9. Shuto, N. & Ti, L.H. (1974), Wave effects on buoyant plumes, Proc. 8th Cong., IAHR, pp.295–300.
10. Yeo, J.H. & Koch, H.J. (1957), Trace analysis , Fluorometer, John Wiley & Sons. Inc.